ACS APPLIED MATERIALS & INTERFACES

Research Article

www.acsami.org

Voltage/pH-Driven Mechanized Silica Nanoparticles for the Multimodal Controlled Release of Drugs

Ting Wang,[†] GuangPing Sun,[†] MingDong Wang,[†] BaoJing Zhou,[‡] and JiaJun Fu*[,†]

[†]School of Chemical Engineering and [‡]Institute of Computation in Molecular and Materials Science and Department of Chemistry, Nanjing University of Science and Technology, Nanjing 210094, P. R. China

Supporting Information

ABSTRACT: The major challenges of current drug delivery systems for combination chemotherapy focus on how to efficiently transport drugs to target sites and release multiple drugs in a programmed manner. Herein, we report a novel multidrug delivery system, MSNPs **1**, based on mechanized silica nanoparticles, which were constructed through functionalization of mesoporous silica nanoparticles with the acid-cleavable intermediate linkages and the monoferrocene functionalized β-cyclodextrin (Fc-β-CD) as supramolecular nanovalves. MSNPs **1** achieved zero premature release in the physiological pH solution and realized two different release modalities. In modality 1, MSNPs **1** released the encapsulated drugs gemcitabine (GEM) and doxorubicin (DOX) in sequence when they were successively applied to voltage and acid stimuli. The release time and dosage of GEM were precisely controlled via external voltage. The subsequent acid-triggered release of DOX was attributed to breakage of the intermediate linkages containing ketal groups. Modality 2 is the concurrent release of these two drugs directly upon acid exposure. Furthermore, the cell viability experiments demonstrated that MSNPs **1** had an improved cytotoxicity to MCF7 cells in comparison with single DOX- or GEM-loaded mechanized silica nanoparticles. We envisage that MSNPs **1** will play an important role in research and development for a new generation of controlled-release drug delivery system.

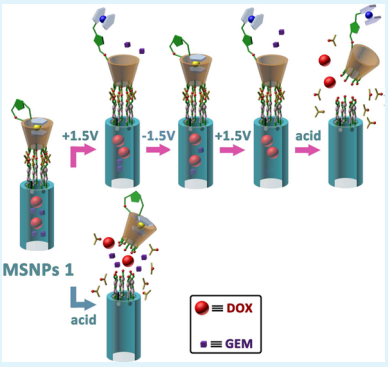

KEYWORDS: *mechanized silica nanoparticles, multimodal controlled release, supramolecular nanovalves, acid-cleavable, voltage stimulation*

INTRODUCTION

Chemotherapy has long been considered as a standard treatment for cancers mainly by using antitumor drugs to inhibit cancer cell proliferation. However, until now, there have been still two major obstacles plaguing researchers and weakening therapeutic efficacy.[1,2] One of the issues is the existence of serious side effects to health cells and tissues due to the poor specificity and high toxicity of cytotoxic drugs. Another complex problem is multidrug resistance (MDR), which is the important defense mechanism for tumor cells and often causes unsatisfactory clinical success or recurrence rate. To overcome these problems, among the advances in the area over the last decades, drug delivery systems for combinations of multiple drugs with different working mechanisms have emerged as one of the most promising and feasible strategic approaches.[3,4] Compared with single-drug chemotherapy, the utilization of multiple drugs can suppress drug resistance and be expected to achieve the synergistic effects. The combination drug therapy definitely placed the higher requirements for multidrug delivery systems (M-DDSs). The ideal M-DDSs should have three essential characteristics: (1) incorporation of multiple drugs into one suitable vehicle; (2) targeted delivery without premature release during blood circulation to avoid side effects; (3) multimodal controlled release of the entrapped drugs. It is highly desired that each drug can be released at setting time, position, and precise dosage in a controlled manner. However, this is still a challenging research topic.

Mechanized silica nanoparticles (MSNPs), composed of mesoporous silica nanoparticles (MSNs) as therapeutic vehicles and supramolecular nanovalves in the form of rotaxanes or pesudorotaxanes anchored on the exterior surface of MSNs, occupy the leading position in the potential candidates for M-DDSs.[5−9] The tunable pore size and large specific surface area of MSNs can accommodate two or more drugs with different molecular sizes only via simple physisorption process and release them independently. More importantly, the critical tasks of zero premature release and multimodal controlled release will be realized by rational design of supramolecular nanovalves, which normally operate by the relative movement of macrocycles on the functionalized linear stalks in response to biological signals (e.g., pH, enzyme)[10−17] and external stimuli (e.g., redox potential, light irradiation, temperature, heating),[18−23] as well as their connection modes with MSNs. Zink and Stoddart put forward the typical M-DDSs based on MSNPs, in which the dual encapsulated cargos were programmed-released after receiving pH and glutathione activations, and whipped up a surge of research interests.[24−27]

Received: June 26, 2015
Accepted: September 8, 2015
Published: September 8, 2015

DOI: 10.1021/acsami.5b05619
ACS Appl. Mater. Interfaces 2015, 7, 21295−21304

Scheme 1. Schematic Illustration of Assembly of MSNPs 1 and the Multimodal Controlled Release of the Two Drugs GEM and DOX

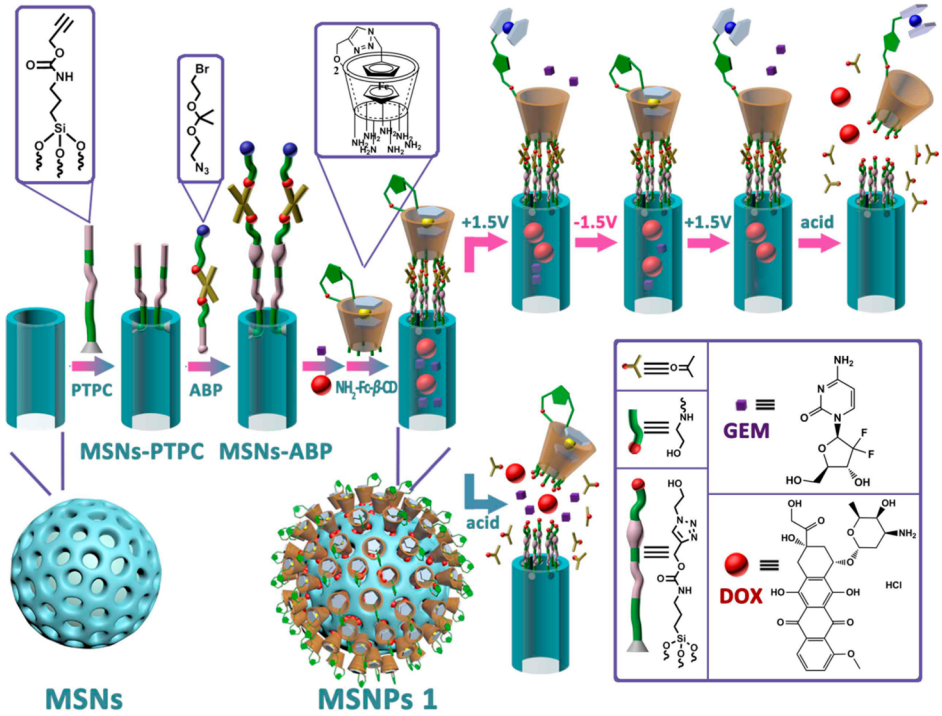

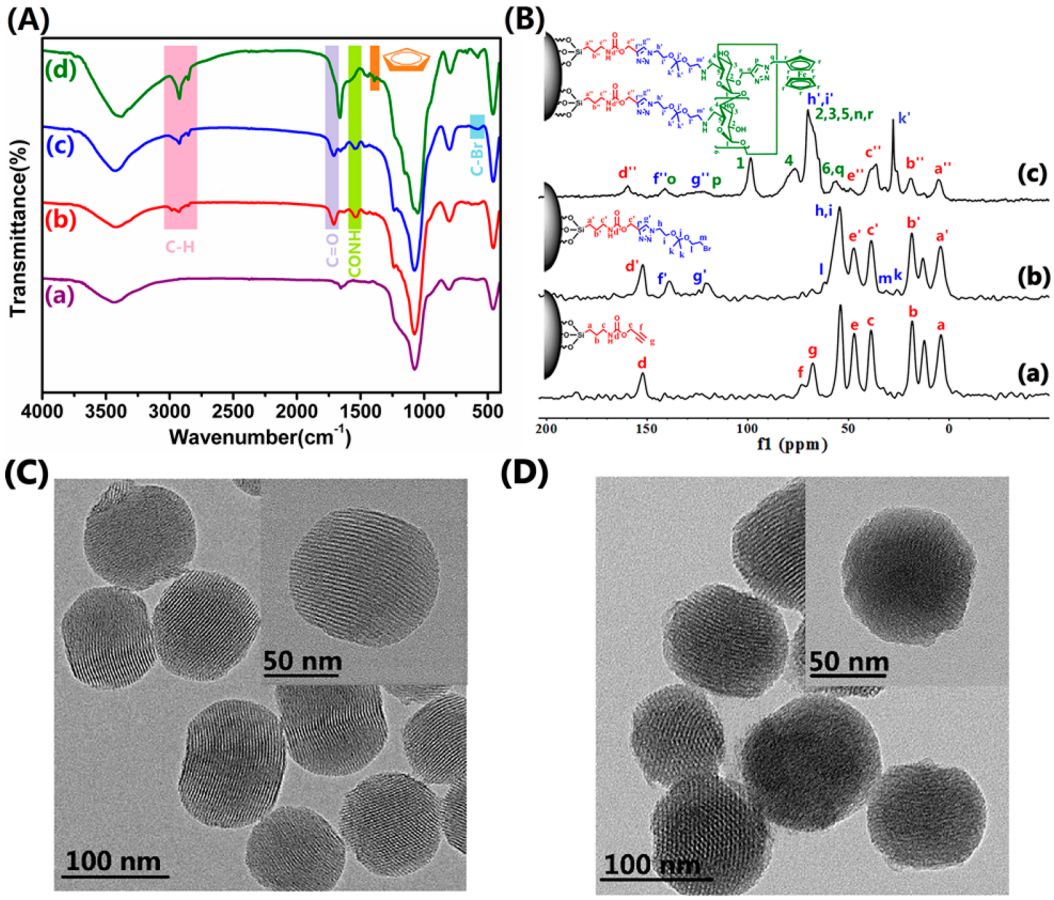

Figure 1. (A) FTIR spectra of (a) MSNs, (b) MSNs−PTPC, and (c) MSNs−ABP, (d) MSNPs **1** (without GEM and DOX). (B) ^{13}C SS-NMR spectra of (a) MSNs−PTPC, (b) MSNs−ABP, and (c) MSNPs **1** (without GEM and DOX). TEM of (C) MSNs and (D) MSNPs **1**.

DOI: 10.1021/acsami.5b05619
ACS Appl. Mater. Interfaces 2015, 7, 21295−21304

Inspired by these works, herein, we designed and fabricated a novel dual stimuli-responsive M-DDS for combination chemotherapy (Scheme 1). The widely used antitumor drugs doxorubicin (DOX) and gemcitabine (GEM) were loaded into the MSNs as model drugs. The specific structure, monoferrocene functionalized β-cyclodextrin (Fc-β-CD) was synthesized as supramolecular nanovalves to show the on/off switch behavior by reversible transition of molecular structure from self-complexation to self-dissociation upon redox potential. β-CD, possessing a hydrophilic exterior surface and hydrophobic interior cavity, is the representative water-soluble macrocycle. On the basis of the fact that the binding affinity between β-CD and some guests (including 1*H*-benzimidazole,[28] polyethylenimine,[29] azobenzene,[30] ferrocene,[31] and methyl orange[24] et al.) incorporated into the stalks are controlled by the external stimuli, pH/light/redox-responsive supramolecular nanovalves have been designed and constructed. However, in most cases, pseudorotaxane-based supramolecular nanovalves cannot reversibly implement "on/off" function due to the dethreading of β-CD from the stalks upon stimuli. In the present work, the assembly of Fc-β-CD is expected to solve this problem. The supramolecular nanovalves and MSNs were connected by acid-cleavable intermediate linkages. The fabricated MSNPs **1** possess two distinct controlled release modalities. In modality 1, when redox potential and acidic stimuli were sequentially applied to MSNPs **1**, GEM and DOX escaped from mesopores of MSNs in sequence. In modality 2, once MSNPs **1** directly encountered the acidic microenvironment, which is the important biological trigger occurring in cancerous tissues, endosomes, or lysosomes, GEM and DOX were released together due to the acidic hydrolysis of ketal groups in the intermediate linkages. In view of the simplicity and practicability of redox potential and pH stimuli, the well-organized MSNPs **1** will adapt to the diverse demands of combination chemotherapy and further improve the therapeutical efficacy.

RESULTS AND DISCUSSION

Preparation and Characterization of MSNPs 1. MSNs, as drug delivery vehicles, with ordered 2D hexagonal mesostructure and average diameter of 100 nm, were prepared according to the previous literature.[32] The specific surface area, pore volume, and BJH pore diameter were 1263 $m^2\ g^{-1}$, 0.97 $cm^3\ g^{-1}$, and 235 nm, respectively (Figure S1 and Table S1, Supporting Information). Prop-2-yn-1-yl (3-(triethoxysilyl) propyl) carbamate (PTPC), 2-(2-azidoethoxy)-2-(2-bromoethoxy) propane (ABP), and mono-2-*O*-[[1-(ferrocenylmethyl)-1*H*-1,2,3-triazol-4-yl]methyl]-heptakis-(6-deoxy-6-amino)-β-cyclodextrin (NH_2-Fc-β-CD), the key components for preparation of MSNPs **1**, were initially synthesized. The synthetic route for MSNPs **1** is depicted in Scheme 1. MSNs were functionalized with PTPC to obtain MSNs−PTPC. The Fourier transform infrared (FTIR) spectrum for MSNs−PTPC (Figure 1A(b)) shows the absorption band at 2933 and 2856 cm^{-1}, belonging to C−H stretching vibrations, and the characteristic adsorption peaks of the amide group at 1709 cm^{-1} ($\nu_{C=O}$) and 1539 cm^{-1} (δ_{N-H}). Furthermore, the ^{13}C solid-state NMR spectrum (^{13}C SS-NMR, Figure 1B(a)) also exhibited the corresponding resonance signals at 4.1 (−Si−**C**H_2−), 18.3 (−Si−CH_2−**C**H_2), 38.8 (−CH_2−**C**H_2−NH−), 47.1 (−O−**C**H_2−), 67.7 (−C≡**C**H), 73.2 (−**C**≡CH), and 152.2 (−**C**=O) ppm. These results demonstrated the grafting of PTPC groups into silica frameworks. Subsequently, MSNs−PTPC were reacted with ABP to yield MSNs−ABP. Compared with MSNs−PTPC, a typical C−Br stretching vibration peak at 529 cm^{-1} was found in the FTIR spectrum of MSNs−ABP (Figure 1A(c)). Meanwhile, in Figure 1B(b), the disappearance of alkynyl signals and the prominent two signals at 139 and 120 ppm, attributed to triazole moieties, were observed. Obviously, ABP groups were immobilized on the exterior surface via Huisgen 1,3-dipolar cycloaddition reaction. After completion of loading with GEM and DOX, NH_2-Fc-β-CD was covalently bonded to MSNs−ABP. To better characterize the last step, GEM and DOX were not included to avoid interference in FTIR and ^{13}C SS-NMR measurements. The peak appearing at 1392 cm^{-1} was assigned to C−H bending vibration in cyclopentadiene, and the strong absorption band at 1661 cm^{-1} owing to O−H bending vibration in β-CD was clearly seen (Figure 1A(d)). In addition, a new series of resonance signals at 70−100 ppm was ascribed to Fc-β-CD portions (Figure 1B(c)). Consequently, MSNPs **1** were completely assembled. The transmission electron microscopy (TEM) images (Figure 1C and D) showed there were no obvious differences in shape and average diameter between MSNs and MSNPs **1**. However, the porous structure of MSNPs **1** became obscure, suggesting surface coverage of the monolayered supramolecular nanovalves.

The step-by-step functionalization processes were also confirmed by N_2 adsorption−desorption isotherm, small-angle X-ray diffraction (SA-XRD), and thermogravimetric analysis (TGA). With the advance of functionalization, the specific surface area, average pore size, and total pore volume persistently decreased (Figure S2 and Table S2, Supporting Information). At the same time, the continuous decrease in intensity of (100) reflection and the gradually vanished peaks at (110) and (200) were clearly seen in the SA-XRD patterns (Figure S3, Supporting Information). Installation of the functional stalks on pore walls and the loading of GEM and DOX in pore channels are responsible for the changing tendency of these parameters. According to the results provided by TGA (Figure S4, Supporting Information) the amount of PTPC, ABP, and NH_2-Fc-β-CD attached on MSNs was calculated as 1.08, 0.448, and 0.071 mmol g^{-1} MSNs, respectively. The TGA results further supported the successful functionalization process.

Sequential Release Modality of MSNPs 1. To investigate the multimodal release triggered by combination of voltage and pH stimuli, fluorescence and UV−vis spectroscopies were used to quantitatively measure the release kinetics of GEM and DOX, respectively. The total amount of entrapped GEM and DOX were calculated to be about 67 and 29 μmol g^{-1} MSNPs **1**, respectively. In the physiological pH solution (PBS, pH = 7.4), the almost flat baselines both in fluorescence and UV−vis spectra at the beginning stage demonstrate there was no uncontrolled leaching of the two drugs, indicating perfect blocking effect of nanovalves on pore outlets. As shown in Figure 2, a progressive release of GEM occurred upon exerting +1.5 V voltage, with the cumulative release reaching 23% loaded GEM over 15 min. Thereafter, the voltage was converted to −1.5 V, the sustained release was gradually ceased, and the remained GEM was reconfined in the mesopores. When the voltage was turned to +1.5 V again, the release process restarted. It is essential that the cyclic "release−halt−release−halt−release" switchable behavior can be easily modulated through redox potential. This interesting release characteristic will precisely control the dosage of GEM

DOI: 10.1021/acsami.5b05619
ACS Appl. Mater. Interfaces 2015, 7, 21295−21304

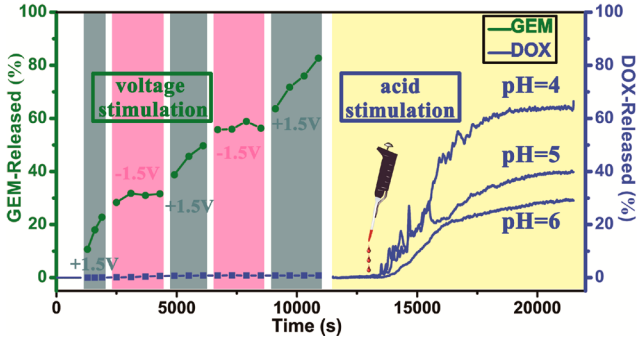

Figure 2. Sequential release profiles of GEM and DOX from MSNPs **1**.

and avoid the drug side effects. It was noteworthy that no obvious fluorescence signal was detected during the whole voltage stimulation process. After removal of electric equipment, the pH solution was adjusted to 6.0, the fluorescence intensity increased with time, and the release amount of DOX was 28% after acidification for 120 min. As the acidity increased from pH 6.0 to 4.0, the release rate of DOX was significantly enhanced. At pH 4.0, 64% of DOX was released within the same time duration. To conclude, MSNPs **1** can release the GEM and DOX in a sequenced fashion upon application to voltage and acid stimuli in turn.

The binding constants between β-CD and ferrocene derivatives are strongly influenced by electrostimulation, hence quite a few molecular machines based on these paramount findings have emerged and captured much attention.[33−36] The study concerning the configurational conversion regularity of Fc-β-CD is the first step to understand the working mechanisms of MSNPs **1**. In aqueous solution, Fc-β-CD is likely to form either a self-complexation at low concentration or an intermolecular association at high concentration.[37,38] To determine the appropriate concentration for keeping self-complexation state, which is also the designed configuration for supramolecular nanovalves, isothermal titration calorimetry (ITC) dilution experiments were performed. From Figure 3A, when Fc-β-CD solution with the concentration of 2.0 mM was added dropwise to the calorimetric cell containing pure water, remarkable endothermic peaks arising from the transformation of intermolecular association into self-complexation were observed in the initial injection stage. The adsorbed heat decreased as the concentration of Fc-β-CD in cell naturally increased. When the concentration was set to 0.1 mM (Figure 3B), in contrast, the negligible heat pulses during the whole dilution process demonstrated that Fc-β-CD originally were in the state of self-complexation and this critical concentration was allowed to reference for surface modification and investigations of nanovalves. The switch behavior of Fc-β-CD was characterized by 2D ROESY NMR spectroscopy. Strong cross correlations between H3/H5 protons at 3.88 and 3.72 ppm of β-CD and cyclopentadiene (Cp or Cp′) region of Fc moieties at the range of 4.2−4.35 ppm are directly visible in Figure 3C, implying the formation of pseudo[1]rotaxane, in which Fc moieties included into the β-CD's cavity via flexible triazole linkers. After oxidation by +1.5 V voltage, Fc moieties were oxidized into ferrocenium (Fc^+) species. The NMR spectroscopy cannot be directly measured due to the paramagnetic nature of Fc^+. Cobaltocenium (Cob^+), an analogue of Fc^+, as alternative was introduced in this work. The 2D ROESY NMR spectrum in

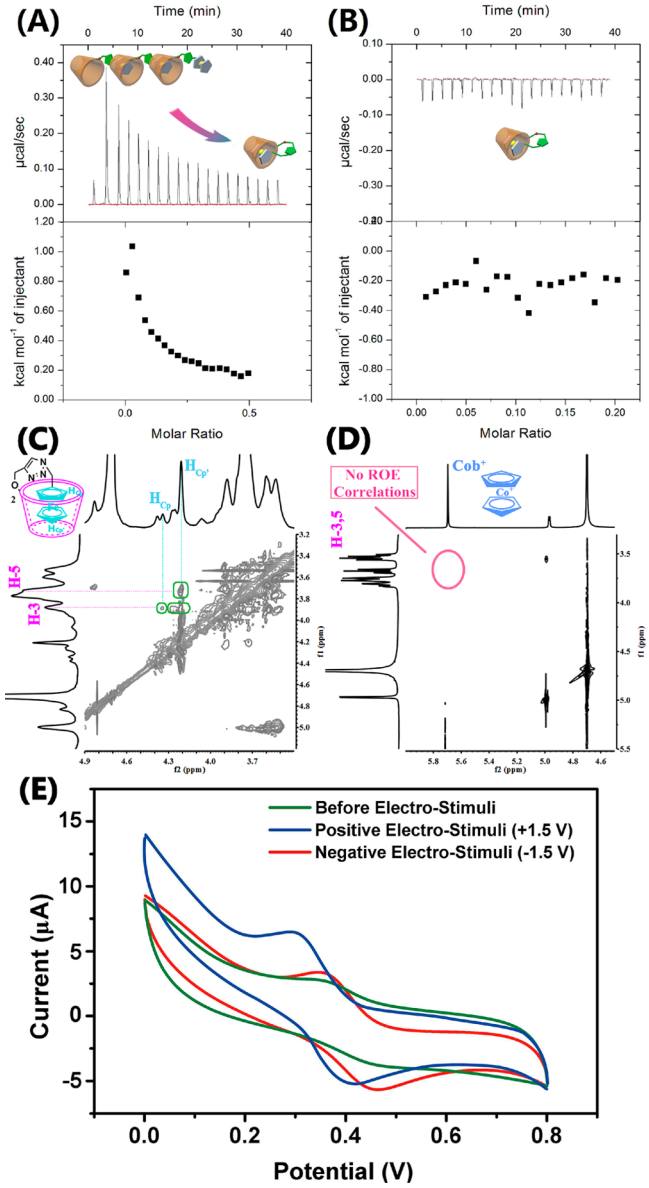

Figure 3. Isothermal titration calorimetry (ITC) data for dilution experiments of Fc-β-CD (A) 2.0 mM, and (B) 0.1 mM comprising the injection of 19 aliquots (2 μL each) into pure water. Partial 2D ROESY spectra (D_2O, 25 °C) of (C) Fc-β-CD (0.1 mM) under psychological pH solution, (D) Cob^+ (0.1 mM) and β-CD (0.1 mM). (E) Cyclic voltammetry experiments for Fc-β-CD (0.1 mM) in PBS (pH 7.4) containing 50 mM NaCl as support.

Figure 3D shows no correlations between protons of Cp/Cp′ and β-CD, inferring that Fc^+ moieties dissociated from β-CD in the structure of Fc^+-β-CD, especially considering certain intramolecular torsional potential energy. Encouragingly, after adjusting the voltage to −1.5 V to Fc^+-β-CD solution, the aggregate was returned to the starting self-complexation state as expected (Figure S5, Supporting Information). The open/closed reversibility of supramolecular nanovalves was further validated by cyclic voltammetry (CV) measurement (Figure 3E). Under PBS (pH 7.4) without electrostimulation, the CV curve of Fc-β-CD solution exhibited a + 0.34 V half-wave potential and the peak current of 2.7 μA. After application of oxidative voltage, the half-wave potential negatively shifted to +0.30 V and the peak current remarkably enhanced to 6.5 μA,

DOI: 10.1021/acsami.5b05619
ACS Appl. Mater. Interfaces 2015, 7, 21295−21304

suggesting that the oxidized Fc^+ moieties excluded from the cavity of β-CD and the self-dissociation of Fc^+-β-CD was definitely formed. Whereas with the subsequent reduction voltage at −1.5 V, the CV curve gradually reverted to its original state, implying the reformation of self-complexation state of Fc-β-CD. Therefore, combined with the ^{1}H NMR and UV−vis absorption data (Figures S6 and S7, Supporting Information), the reversible supramolecular nanovalves shoulder the mission of the voltage-responsive controlled release of GEM. Unlike the previously reported supramolecular nanovalves based on pseudorotaxane,[39−42] the repeated intramolecular configuration transformations avoid the detachment of macrocycles from the stalks and realize the multistage release of GEM at precise dosage and time in a controlled manner. On the other hand, in comparison with DOX, GEM possesses the smaller molecular volume, which is beneficial to the effusion from cavity of β-CD. The binding constant between GEM and β-CD theoretically calculated by molecular dynamics/quantum chemistry/continuous solution model (MD/QM/CSM; the detailed calculation method and results can be seen in the Supporting Information, Figure S8 and Table S3) is lower than that between β-CD and p-coumalic acid, which has also been proved to be capable of flowing out of the cavity.[24,32] These results guarantee GEM concentration-diffusion through the cavity with ease. The control experiment I was carried out to get insight into the Fc moieties as the role of gatekeepers for GEM. MSNPs **2** were constructed following the same procedure as MSNPs **1**, except for employing NH_2-β-CD to replace NH_2-Fc-β-CD (Figure 4A; the detailed synthetic procedure can be seen in the Supporting Information). No matter what voltages were imposed in the release experiment, the UV−vis signal around λ = 267 nm shows no switchable behavior (Figure 4B), indicating the key role of Fc moieties for

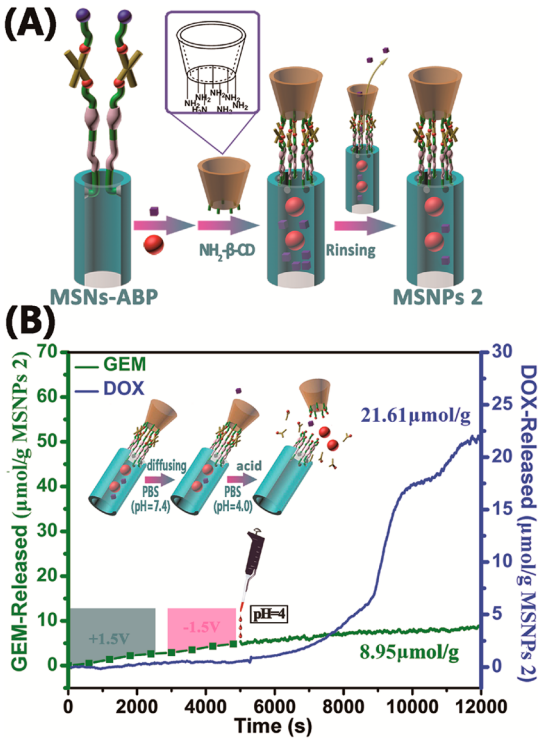

Figure 4. (A) Construction of MSNPs **2** and (B) release profiles of GEM and DOX from MSNPs **2**.

voltage-stimulus controlled release of GEM. Furthermore, the total amount of GEM remaining in nanopores was lower than that in MSNPs **1**, which could be attributed to the fact that, without the plugging of Fc moieties, a majority of GEM was washed off during the preparation of MSNPs **2**.

The pH-controlled release of DOX was attributed to the intermediate linkages bearing ketal groups. Drug delivery platforms based on the ketal groups have some advantages, such as high sensitivity to acidic environment of tumors and the ease of excretion of degradation products including alcohol and acetone. Under the acidic circumstance, MSNPs **1** were cleaved into two main fragments: the DOX-loaded MSNs conjugated with the incomplete stalks and the detached NH_2-Fc-β-CD portion (Scheme 1). The loss of β-CD caps resulted in the release of DOX from MSNs. In light of the mechanism of ketal hydrolysis catalyzed by acid substances, it was not difficult to understand that the rate of cleavage of the ketal linker increased as the pH decreased, which explained the pH-dependent release rate of DOX shown in Figure 2. Moreover, Fc moieties had no effects on the pH-triggered release of DOX (Figure 4B). The MD/QM/CSM method was also performed to find the binding mode of β-CD and DOX. However, no binding mode was generated due to the limitation of molecular size (Figure S8, Supporting Information). DOX was sealed either in MSNPs **1** or in MSNPs **2** by β-CD caps, indicating that DOX of large molecular volume cannot pass through the cavity of β-CD freely. This phenomenon was also reported in some previous literature.[43,44]

Concurrent Release Modality of MSNPs 1. To illustrate the controlled release modality 2, the order of the external stimuli was reversed. After being located in acidic solution, MSNPs **1** exhibited a simultaneously sustained DOX/GEM release behavior (Figure 5A). The percentage of drug release from the MSNPs **1** after 2.5 h achieved 92% and 69% for GEM and DOX, respectively. The release rates for the two drugs were also dominated by the pH values, which was in keeping with the splitting rate of intermediate linkages. Significantly, when MSNPs **1** were first treated with acidic attack, the later voltage stimulus could not regulate the flow stream of GEM again. For most MSNPs, it is arduous to prevent premature release of drugs with relative small molecular volume from the gaps between supramolecular nanovalves and MSNs. The length and the installation locations of stalks are usually cautiously taken into account.[45] In our experiment, there are two reasons behind the excellent blocking effect of GEM under normal condition. First, Fc-β-CD undertakes the gatekeeper task to vertically lock well. Second, one Fc-β-CD has seven tentacles at the C6 position to connect with the functionalized MSNs, which form the cage-like structure and increase the horizontal steric hindrance for out-diffusion. To certify our hypothesis, control experiment II was conducted. MSNs were functionalized with PTPC, ABP, and mono-NH_2-Fc-β-CD to assemble MSNPs **3** (Figure 5B; the detailed synthetic procedure can be seen in the Supporting Information). Because of only one tentacle at C6 position, the intermediate linkage density per unit area over every mesoporous orifice for MSNPs **3** is considerably lower than that for MSNPs **1**. GEM crept out from the loose barrier fences of MSNPs **3** even in the presence of "closed" Fc-β-CD during the preparation process, which caused the remained amount of GEM in MSNPs **3** to be only about 6.0 μmol g^{-1} MSNPs **3** (Figure 5C). Because of the lack of protection for gaps, MSNPs **3** could not execute controlled release, and the residual GEM diffused out of MSNPs **3** by concentration

DOI: 10.1021/acsami.5b05619
ACS Appl. Mater. Interfaces 2015, 7, 21295−21304

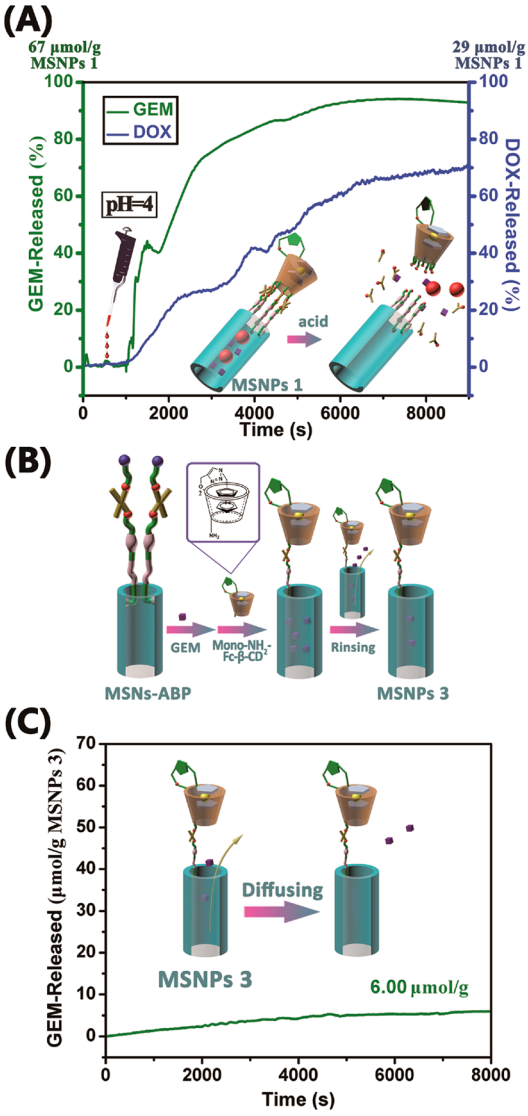

Figure 5. (A) Concurrent release profiles of GEM and DOX from MSNPs **1**. (B) Construction of MSNPs **3**. (C) Release profile of GEM from MSNPs **3**.

gradient. As far as MSNPs **1** are concerned, the irreversible ketal hydrolysis process leads to the results that the cavities of β-CD are not the only export channel for GEM and thus the voltage stimulus loses its effectiveness.

Cytotoxicity Assay. After completing controlled-release experiments, the in vitro cytotoxicity of MSNPs **1** against MCF7 cells was further investigated by MTT assay, an approach widely used for quantitative testing of cell viability. As shown in Figure 6, unloaded MNSPs **1** showed no obvious cytotoxic effects on MCF7 cells in the range of 3−100 μg mL^{-1} after incubation for 48 h. At the concentration of 100 μg mL^{-1}, the cell viability was about 85%, indicating the excellent biocompatibility of empty MSNPs **1** as drug vehicles. In contrast, a considerable decrease in cancer cell viability was observed when MCF7 cells were incubated with MSNPs **1**. The cell viability was only 20% after incubation by MSNPs **1** (100 μg mL^{-1}; the equivalent dosage: 1.76 μg mL^{-1} (GEM) and 1.68 μg mL^{-1} (DOX)) for 48 h. Combined with the specific controlled-release feature of MSNPs **1**, it is conceivable that MSNPs **1** will maintain negligible premature release during

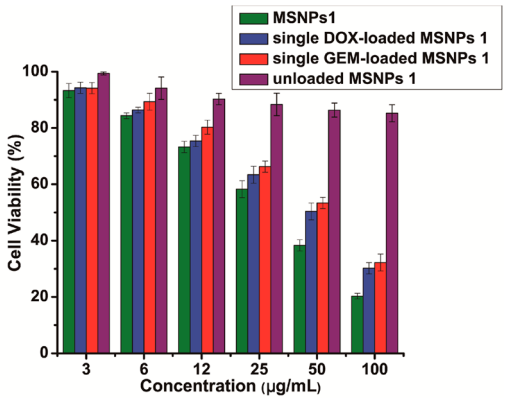

Figure 6. Viability of MCF7 cells incubated with MSNPs **1**, single-DOX-loaded MSNPs **1**, single-GEM-loaded MSNPs **1**, and unloaded MSNPs **1** at different nanoparticles concentrations.

blood circulation (pH 7.4) while accomplishing co-release of DOX and GEM upon reaching tumor cells, where the acidic microenvironments occurring in endosomes (pH 5.0−6.5) and lysosomes (pH 4.5−5.0) are believed to be reliable triggers to release drugs.[39] To horizontally compare the cytotoxicity efficacy, we individually incubated single-GEM-loaded MSNPs **1** and single-DOX-loaded MSNPs **1**, in which the total amount of encapsulated single drug (~35 mg GEM or DOX g^{-1} MSNPs **1**) was basically at the same level as MSNPs **1** (17.6 mg GEM + 16.8 mg DOX g^{-1} MSNPs **1**) through adjustment of loading conditions, at different concentration with MCF7 cells. Under the identical concentration, the cell viability of MSNPs **1** was lower than that for two single-drug-loaded MSNPs **1**, revealing the synergistic effectiveness to kill cancer cells and exhibiting the potential application in combination therapy to overcome cancer multidrug resistance.

CONCLUSIONS

In summary, the novel drug delivery platform based on mechanized silica nanoparticles, consisting of MSNs vehicles, acid-cleavage intermediate linkages, and reversible supramolecular nanovalves, were devised and achieved multimodal controlled release of two drugs. By arranging the orders of external stimuli, GEM and DOX were controlled-released from MSNPs **1** not only in sequential modality but also in concurrent modality. In addition, MSNPs **1** are expected to accommodate the other drugs for multimodal controlled release. It is necessary to note that the molecular size of the drugs and the binding affinity between the drugs and β-CD should be primarily considered. We envision that the MSNPs **1** described here will provide a new option for smart M-DDSs and have great application for combination chemotherapy. Our future work will focus on the application of MSNPs **1** for tumor-targeted combination chemotherapy in vivo.

EXPERIMENTAL SECTION

Materials and Methods. All chemicals were purchased from Sigma-Aldrich and Aladdin Industrial Inc. (Shanghai, China) (the detailed materials can be seen in the Supporting Information). The reagents were of analytical grade and used as received. ^{1}H, ^{13}C, and 2D ROESY NMR spectra were recorded on a Bruker AVANCE 300 spectrometer. Mass spectra were recorded on a Thermo Trace DSQ LC-MS spectrometer. The ^{13}C CP-MAS solid-state NMR (^{13}C SS-NMR) spectra were obtained on a Bruker AVANCE III WB 400 NMR spectrometer using 4-mm ZrO_2 rotors spinning at 12 kHz, and Larmor frequency was set to 79.5 MHz. Transmission electron microscopy

DOI: 10.1021/acsami.5b05619
ACS Appl. Mater. Interfaces 2015, 7, 21295−21304

(TEM) images were taken using a JEM-2100 microscope (100 kV). The samples were prepared by dispersing the powder in acetone, followed by dropping the suspension onto a Cu grid covered by carbon film. Fourier transform infrared spectrophotometer (FTIR) analyses were collected by a Bruker Tensor 27 FTIR spectrometer. Small-angle powder X-ray diffraction (SA-XRD) measurements were carried out on a Bruker D8 Advanced diffractometer applying monochromatized Cu Kα radiation. The textural properties of the materials were estimated by N_2 adsorption−desorption isotherms at −196 °C (Quanta chrome Nova 1000 Micrometric apparatus). The specific surface areas were calculated by applying the Brunauer−Emmett−Teller (BET) equation, and the pore size distributions were calculated using the BJH model. Thermogravimetric analysis (TGA) measurements were performed with a Mettler TGA-SDTA 851e instrument with a heating rate of 20 °C min^{-1} in nitrogen flow. Isothermal titration calorimetry (ITC) experiments were carried out using a Malvern MicroCal ITC200 apparatus. UV/vis absorption spectra and fluorescence spectra were obtained over time on a Shimadzu UV-1800 spectrometer and a Shimadzu RF-5201 spectrophotometer, respectively. CV experiments were performed by using a platinum sheet working electrode. The electrode surface was immersed in a 50% v/v H_2SO_4 solution for 5 min and rinsed with distilled water immediately before use. The counter electrode was a glassy carbon electrode and the reference electrode was a Ag/AgCl electrode. The concentration of the supporting electrolyte sodium chloride was set to 0.1 M.

Preparation of MSNs. CTAB (0.6 g) was first dissolved in deionized water (240 mL). Sodium hydroxide (aq. 2.0 M, 1.75 mL) was added to CTAB solution, followed by raising the solution temperature to 80 °C. The mixture was stirred for 3 h after adding TEOS (2.5 mL) dropwise. The crude product was collected by filtration, washed with deionized H_2O and MeOH, and then dried in air. Finally, CTAB was removed by refluxing the crude product (0.55 g) in the mixture of 2-propanol (100 mL) and HCl (aq. 37%, 10 mL) to give MSNs for further use.

Synthesis of Prop-2-yn-1-yl [3-(triethoxysilyl) propyl] Carbamate (PTPC; the Detailed Synthetic Procedure Can Be Seen in the Supporting Information). A solution of 3-isocyanatopropyl triethoxysilane (ICPTES, 4.5 mL, 18.1 mmol) in dichloromethane (5 mL) was added dropwise to a stirred solution of propargyl alcohol (1.2 mL, 20.8 mmol) and triethylamine (2.4 mL, 17.2 mmol) in dichloromethane (10 mL) in an ice bath. The resulting solution was stirred overnight at room temperature. Afterward, the mixture was poured into distilled water, extracted with dichloromethane, dried over anhydrous Na_2SO_4 ,and concentrated in vacuo to give PTPC (4.6 g, yield 83%). ^{1}H NMR (300 MHz, $CDCl_3$) δ 5.06 (s, 1H, NH), 4.66 (d, J = 2.3 Hz, 2H, CH_2CC), 3.81 (q, J = 7.0 Hz, 6H, OCH_2), 3.19 (dd, J = 13.0, 6.6 Hz, 2H, CH_2N), 2.45 (t, J = 2.4 Hz, 1H, CCH), 1.74−1.51 (m, 2H, CCH_2C), 1.22 (t, J = 7.0 Hz, 9H, CH_3), 0.72−0.52 (m, 2H, CH_2Si). ^{13}C NMR (75 MHz, $CDCl_3$) δ 156.39 (NCOO), 79.55 (C), 75.52 (CH), 59.49 (OCH_2), 53.30 (OCH_2C), 44.51 (NCH_2), 24.18 (CCH_2C), 19.30 (CH_3), 8.55 ($SiCH_2$). MS (ESI): m/z calcd for $C_{13}H_{25}NO_5Si$, 303.15; found, 326.15 $[M + Na]^+$.

Synthesis of 2-(2-azidoethoxy)-2-(2-bromoethoxy) Propane (ABP; the Detailed Synthetic Procedure Can Be Seen in the Supporting Information). *2,2-bis (2-bromoethoxy) Propane (Compound 1).* 2-Bromoethanol (5.0 mL, 71.6 mmol) and 2,2-dimethoxypropane (4.0 mL, 32.4 mmol) were dissolved in benzene (16 mL), and p-toluenesulfonic acid (5.0 mg, 0.029 mmol) as catalyst was added. The mixture was stirred at 60 °C for 12 h and then cooled to room temperature. Sodium methoxide (100 mg, 1.85 mmol) in methanol (2 mL) was then injected and the temperature of the mixture was raised to collect the fraction at 85 °C. The crude product was poured into DMF (50 mL) and extracted with hexane (3 × 150 mL). The combined organic phase was washed with brine, dried over anhydrous Na_2SO_4, and concentrated in vacuo to give Compound **1** (6.9 g, yield 73%). ^{1}H NMR (300 MHz, $CDCl_3$) δ 3.81 (t, J = 3.7 Hz, 4H, OCH_2), 3.46 (t, J = 3.7 Hz, 4H, $BrCH_2$), 1.40 (s, 6H, CH_3). ^{13}C NMR (75 MHz, $CDCl_3$) δ 98.59 (C), 61.64 (OCH_2), 40.87 ($BrCH_2$), 23.79 (CH_3).

ABP. A solution of Compound **1** (1.028 g, 3.5 mmol), sodium azide (230 mg, 3.5 mmol), and TBAB (56.4 mg, 0.17 mmol) in anhydrous DMF (25 mL) was stirred at room temperature for 3 days. After completion of the reaction, the reaction mixture was poured into water and extracted with dichloromethane (3 × 40 mL). The combined organic phase was washed with brine, dried over anhydrous Na_2SO_4, and concentrated in vacuo. The crude product was purified by column chromatography over silica gel using hexane/ethyl acetate (6:1) as the eluant to afford ABP (0.66 g, yield 75%). ^{1}H NMR (300 MHz, $CDCl_3$) δ 3.81 (d, J = 3.2 Hz, 2H, OCH_2CBr), 3.66 (dd, J = 5.1, 2.0 Hz, 2H, CH_2Br), 3.47 (d, J = 3.9 Hz, 2H, OCH_2CN_3), 3.37 (m, 2H, CH_2N_3), 1.41 (s, 6H, CH_3). ^{13}C NMR (75 MHz, $CDCl_3$) δ 99.40 (C), 60.26 ($OCCN_3$), 58.97 ($OCCBr$), 49.87 (CN_3), 30.04 (CBr), 23.64 (CH_3).

Synthesis of mono-2-O-{[1-(ferrocenylmethyl)-1H-1,2,3,triazol-4-yl]methyl}-heptakis(6-deoxy-6-amino)-β-Cyclodextrin (NH_2-Fc-β-CD; the Detailed Synthetic Procedure Can Be Seen in the Supporting Information). *Mono-2-O-propargyl-β-CD (Compound 2).* To a stirred solution of β-CD (1 g, 0.881 mmol) in anhydrous DMSO (15 mL) was added lithium hydride (11 mg, 1.322 mmol) under nitrogen atmosphere. After being stirred at room temperature for 24 h, the suspension became clear. A mixture of propargyl bromide in toluene (80 wt %, 98 μL, 0.881 mmol) and a small amount of lithium iodide were then added, and the reaction was stirred at 55 °C in the darkness for another 5 h. The reaction mixture was then poured into acetone (300 mL), and the precipitate was filtered and thoroughly washed with acetone. The crude product was purified by silica gel chromatography (10:5:2 CH_3CN:H_2O:NH_4OH) to afford Compound **2** (308 mg, yield 29%). ^{1}H NMR (300 MHz, DMSO-d_6) δ 5.80 (dddd, J = 17.5, 12.2, 10.9, 3.9 Hz, 11H, OH), 4.98 (d, J = 1.9 Hz, 1H, H-1^A), 4.82 (s, 6H, H-1), 4.54−4.50 (m, 1H, CH_2), 4.50−4.44 (m, 9H, OH), 4.40 (dd, J = 9.5, 1.3 Hz, 2H, CH_2), 3.78 (t, J = 5.6 Hz, 1H, H-3^A), 3.77−3.52 (m, 27H, H-3, 5, 6, 6′), 3.50 (t, J = 1.3 Hz, 1H, ≡CH), 3.45−3.39 (m, 2H, H-2^A, 4^A), 3.40−3.26 (m, H-2, 4, HDO). ^{13}C NMR (75 MHz, DMSO-d_6) δ 102.03−101.77 (C-1), 100.18 (C-1^A), 82.26−81.53 (C-4), 79.94 (C≡), 79.18 (C-2^A), 77.86 (≡CH), 73.12−71.80 (C-2, 3, 5), 59.99 (C-6), 58.80 (CH_2). MS (ESI): m/z calcd for $C_{45}H_{72}O_{35}$: 1172.35; found, 1195.55 $[M + Na]^+$.

Azidomethylferrocene (Compound 3). A solution of ferrocenemethanol (50 mg, 0.231 mmol), acetic acid (3 mL), and sodium azide (90.3 mg, 1.39 mmol) was heated at 50 °C under nitrogen atmosphere for 3 h. After being cooled to the room temperature, the mixture was poured into dichloromethane (50 mL). The combined organic phase was washed with saturated $NaHCO_3$ solution (3 × 50 mL) and distilled water (1 × 50 mL), dried over anhydrous Na_2SO_4, and concentrated in vacuo to give Compound **3** (50 mg, yield 90%). ^{1}H NMR (300 MHz, $CDCl_3$) δ 4.24 (d, J = 1.6 Hz, 2H), 4.20 (d, J = 1.6 Hz, 2H), 4.17 (s, 5H), 4.12 (s, 2H). ^{13}C NMR (75 MHz, $CDCl_3$) δ 81.96 (C), 68.64 (C_{Cp}), 68.53 (C_{Cp}), 50.79 (CH_2N_3).

Iodo (triethyl phosphite) Copper (Compound 4). To a solution of triethyl phosphite (5.52 mL, 31.6 mmol) in benzene (30 mL) was added copper iodide (6 g, 31.6 mmol), and the reaction was stirred at room temperature in the darkness for 1 h. The reaction mixture was concentrated in vacuo, and the crude product was recrystallized from cyclohexane to give Compound **4** (4 g, yield 36%). ^{1}H NMR (300 MHz, DMSO-d_6) δ 4.06−3.96 (m, 6H, CH_2), 1.21 (t, J = 7.0 Hz, 9H, CH_3). ^{13}C NMR (75 MHz, DMSO-d_6) δ 59.73 (CH_2), 16.39 (CH_3).

Mono-2-O-{[1-(ferrocenylmethyl)-1H-1,2,3-triazol-4-yl]methyl}-β-cyclodextrin (Fc-β-CD). To a solution of Compound **2** (300 mg, 0.256 mmol) and Compound **4** (18 mg, 0.05 mmol) in DMF (10 mL) was added Compound **3** (68 mg, 0.282 mmol), and the reaction was stirred at 105 °C for 5 h under nitrogen atmosphere. The reaction mixture was poured into acetone (200 mL), and the precipitate was filtered and washed with acetone thoroughly to afford Fc-β-CD (347 mg, yield 96%). ^{1}H NMR (300 MHz, DMSO-d_6) δ 8.07(s, 1H, H5−C_2HN_3), 5.92 (brs, 2H, OH), 5.78−5.69 (m, 10H, OH), 5.29 (d, J = 9.3 Hz, 2H, CHN), 4.87−4.84 (m, 8H, H1, CHO), 4.78 (d, J = 7.6 Hz, 1H, CHO), 4.63 (brs, 1H, OH), 4.52 (s, 1H, OH), 4.47−4.43 (m, 6H, OH), 4.35 (brs, 2H, H_{Cp}), 4.21 (s, 5H, $H_{Cp'}$), 4.19 (s, 2H, H_{Cp}), 3.85 (t, J = 5.6 Hz, 1H, H3^A), 3.65−3.56 (m, 27H, H-3, 5, 6, 6′), 3.43 (m,

DOI: 10.1021/acsami.5b05619
ACS Appl. Mater. Interfaces 2015, 7, 21295−21304

2H, H-2^A, H-4^A), 3.41−3.35 (m, H-2, 4, HDO). ^{13}C NMR (75 MHz, DMSO-d_6) δ 143.65 (C4−C_2HN_3), 123.81 (C5−C_2HN_3), 102.17 (C-1), 100.26 (C-1^A), 82.43 (C), 82.21−81.67 (C-4), 79.90 (C-2^A), 73.21−72.26 (C-2, C-3, C-5), 72.41 (C-3^A), 68.79 ($C_{Cp'}$), 67.71(C_{Cp}), 64.50 (CH_2O), 60.08 (C-6), 49.25 (CH_2N). MS (ESI): m/z calcd for $C_{56}H_{83}N_3O_{35}Fe$: 1413.42; found, 1436.41 $[M + Na]^+$.

Mono-2-O-{[1-(ferrocenylmethyl)-1H-1,2,3-triazol-4-yl]methyl}-heptakis(6-deoxy-6-iodo)-β-cyclodextrin (Compound 5). A solution of Fc-β-CD (0.622 g, 0.44 mmol), triphenylphosphine (2.308 g, 8.8 mmol), iodine (2.234 g, 8.8 mmol), and anhydrous DMF (9 mL) was stirred under nitrogen atmosphere at 70 °C for 18 h. After the reaction was cooled to room temperature, a solution of sodium methoxide (0.56 g) in methanol (8 mL) was added dropwise under nitrogen atmosphere and the reaction was allowed to stir for 1 h. The reaction mixture was poured into methanol (60 mL), and the precipitate was filtered, washed with methanol, and concentrated in vacuo to afford Compound **5** (239 mg, yield 25%). ^{1}H NMR (300 MHz, DMSO-d_6) δ 8.13 (s, 1H, H5−C_2HN_3), 5.95 (m, 12H, OH), 5.32 (d, J = 15.5 Hz, 2H, CHN), 5.12−4.85 (m, 9H, H1, CHO), 4.53 (brs, 2H, H_{Cp}), 4.18 (s, 5H, $H_{Cp'}$), 4.15 (s, 2H, H_{Cp}), 3.79 (t, J = 9.4 Hz, 1H, H3^A), 3.59 (m, 27H, H-3, 5, 6, 6′), 3.36 (m, H-2, 4, HDO). ^{13}C NMR (75 MHz, DMSO-d_6) δ 143.65 (C4−C_2HN_3), 128.85 (C5−C_2HN_3), 102.09 (C-1), 100.58 (C-1^A), 83.08 (C), 82.82−81.72 (C-4), 79.83 (C-2^A), 73.48−70.98 (C-2, C-3, C-5), 72.08 (C-3^A), 68.62 ($C_{Cp'}$), 68.37 (C_{Cp}), 64.46 (CH_2O), 49.28 (CH_2N), 9.32 (C-6).

Mono-2-O-{[1-(ferrocenylmethyl)-1H-1,2,3-triazol-4-yl]methyl}-heptakis(6-deoxy-6-azido)-β-cyclodextrin (Compound 6). To a solution of Compound **5** (0.343 g, 0.157 mmol) in anhydrous DMF (5 mL) was added sodium azide (0.1 g, 1.538 mmol). The reaction was stirred at 60 °C under nitrogen for 20 h. The reaction mixture was concentrated in vacuo, and the crude product was washed with distilled water, collected by centrifugation, and recrystallized from ethanol to give Compound **6** (200 mg, yield 80%). ^{1}H NMR (300 MHz, DMSO-d_6) δ 7.59 (s, 1H, H5−C_2HN_3), 5.90−5.78 (m, 12H, OH), 5.30 (d, J = 15.5 Hz, 2H, CHN), 4.91−4.90 (m, 9H, H1, CHO), 4.53 (brs, 2H, H_{Cp}), 4.28 (s, 5H, $H_{Cp'}$), 4.23 (s, 2H, H_{Cp}), 3.73 (t, J = 9.4 Hz, 1H, H3^A), 3.60 (m, 27H, H-3, 5, 6, 6′), 3.34 (m, H-2, 4, HDO). ^{13}C NMR (75 MHz, DMSO-d_6) δ 136.48 (C4−C_2HN_3), 135.48, 134.77, 133.62, 133.06, 131.64, 130.37 (C5−C_2HN_3), 103.60 (C-1), 85.71 (C), 84.73 (C-4), 80.96 (C-2^A), 74.13−70.10 (C-2, C-3, C-5), 71.86 (C-3^A), 52.83 (C-6).

NH_2-Fc-β-CD. To the solution of Compound **6** (243 mg, 0.153 mmol) in anhydrous DMF (4 mL) was added triphenylphosphine (636 mg, 2.42 mmol), and the reaction was stirred at room temperature for 1 h under nitrogen atmosphere. Concentrated aqueous ammonia (28%, 2.25 mL) was then added dropwise within 5 min. After being stirred for 18 h at room temperature, the reaction mixture was concentrated in vacuo, and the residue was poured into ethanol. The precipitate was filtered and evaporated in vacuo to give NH_2-Fc-β-CD (172 mg, yield 80%). For NMR measurement, NH_2-Fc-β-CD was converted to amine salt by addition of a dilute solution of DCL (down to pH 6). ^{1}H NMR (300 MHz, D_2O) δ 7.70 (s, 1H, H5−C_2HN_3), 5.02 (m, 9H, H1, CHO), 4.40 (brs, 9H, H_{Cp}, $H_{Cp'}$), 4.05 (t, J = 9.4 Hz, 7H, H-1), 3.83 (m, 7H, H-6′), 3.52 (m, 14H, H-3, 5), 3.44 (dd, 14H, H-2, 4), 3.28 (dd, 7H, H-6). ^{13}C NMR (75 MHz, D_2O) δ 101.20 (C-1), 81.93 (C-4), 80.41 (C-2^A), 71.84−71.29 (C-2, C-3, C-5), 70.82 (C-3^A), 39.82 (C-6). MS (ESI): m/z calcd for $C_{56}H_{90}FeN_{10}O_{28}$, 140; found, 1408.88 $[M + H]^+$.

Preparation of MSNPs 1. *MSNs−PTPC.* MSNs (200 mg) were dispersed in anhydrous toluene (10 mL). PTPC (100 μL, 0.326 mmol) was then added dropwise to the suspension. The reaction mixture was refluxed under nitrogen atmosphere for 24 h. MSNs−PTPC was isolated by centrifugation and washed with methanol and toluene several times.

MSNs−ABP. MSNs−PTPC (200 mg) were suspended in anhydrous DMF (10 mL). ABP (100 mg, 0.397 mmol) and Compound **4** (25 mg, 0.07 mmol) were then added to the suspension. The mixture was stirred under nitrogen atmosphere at 110 °C for 24 h. The resulting materials were centrifuged, washed with DMF and methanol thoroughly, and dried in vacuo overnight to obtain MSNs−ABP.

MSNPs 1. MSNs−ABP (20 mg) were dispersed in the phosphate buffer saline (PBS; pH = 7.4, 50 mL) containing GEM (50 mg) and DOX (5 mg), and the suspension was stirred at 40 °C for 24 h. K_2CO_3 (12 mg, 0.08 mmol), KI (14 mg, 0.08 mmol), and NH_2-Fc-β-CD (16.4 mg, 0.012 mmol) were then added to the suspension and stirred for another 24 h. The nanoparticles were collected by centrifugation, washed with PBS (pH 7.4), and dried in vacuo overnight to yield MSNPs **1**.

Release Experiments. The amounts of released GEM and DOX in the supernatant were monitored by UV/vis spectroscopy (λ = 267 nm) and fluorescence spectroscopy (λ_{ex} = 470 nm, λ_{em} = 554 nm), respectively, and analyzed with a standard calibration curve experimentally obtained. As for voltage stimulation, the release experiments were performed with a three electrode setup consisting of platinum sheet as working electrode, a platinum foil as counter electrode, and a Ag/AgCl (3 M KCl) as reference electrode. MSNPs **1** (5 mg) were directly drop-casted on working electrode. To investigate the voltage-stimuli triggered release of MSNPs **1**, the voltage was oxidized at +1.5 V vs SHE and reduced at −1.5 V vs SHE in PBS solution (40 mL, PBS 7.4). An aliquot of the supernatant was withdrawn at predetermined time intervals to determine the concentrations of GEM and DOX. For acid-stimulation, MNSPs **1** were sealed in the dialysis bag (MWCO 8000 Da) and placed at the top of the quart cuvette to avoid particle interference. PBS (3.8 mL, pH7.4) was added into the cuvette to ensure that MSNPs **1** were immersed into the solution. Continuous-monitoring UV/vis and fluorescence spectroscopic methods were used to determine the concentrations of GEM and DOX, respectively.

Cytotoxicity Assay. The cytotoxicity assay was evaluated by an MTT assay in MCF7 cells (human breast adenocarcinoma cell line). MCF7 cells in culture medium were seeded into a 96-well plate at a 8000 cells per well at 37 °C under 5% CO_2 to allow stabilization. After growing overnight, the cells were then incubated with the unloaded MSNPs **1**, MSNPs **1**, or single-drug-loaded MSNPs **1** with various concentrations for 48 h, respectively. MTT solution (20 μL, 5 mg mL^{-1}) was then added to each well. After another 4 h incubation, the medium was withdrawn and 150 μL of DMSO was added to dissolve the precipitated formazan violet crystals. The absorbance of each sample was measured at 490 nm by a microplate reader (Bio-Rad model 680). All the tests were performed in triplicate.

■ ASSOCIATED CONTENT

Ⓢ Supporting Information

The Supporting Information is available free of charge on the ACS Publications website at DOI: 10.1021/acsami.5b05619.

2D ROESY NMR, ^{1}H NMR, and UV−vis spectra of Fc-β-CD. Theoretical calculation methods for binding affinity between β-CD and guests. (PDF)

■ AUTHOR INFORMATION

Corresponding Author

*E-mail: fujiajun668@gmail.com.

Notes

The authors declare no competing financial interest.

■ ACKNOWLEDGMENTS

We thank the Fundamental Research Funds for the Central Universities, 30915011312, 2013-ZiJin-0102 Talent Program, NUST, QingLan Project, Jiangsu Province, China and A project funded by the Priority Academic Program Development of Jiangsu Higher Education Institutions (PAPD).

■ REFERENCES

(1) Iyer, A. K.; Singh, A.; Ganta, S.; Amiji, M. M. Role of Integrated Cancer Nanomedicine in Overcoming Drug Resistance. *Adv. Drug Delivery Rev.* **2013**, *65*, 1784−1802.

DOI: 10.1021/acsami.5b05619
ACS Appl. Mater. Interfaces 2015, 7, 21295−21304

(2) Brigger, I.; Dubernet, C.; Couvreur, P. Nanoparticles in Cancer Therapy and Diagnosis. *Adv. Drug Delivery Rev.* **2012**, *64*, 24−36.
(3) Zhang, Y.; Chan, H. F.; Leong, K. W. Advanced Materials and Processing for Drug Delivery: the Past and the Future. *Adv. Drug Delivery Rev.* **2013**, *65*, 104−120.
(4) Creixell, M.; Peppas, N. A. Co-Delivery of siRNA and Therapeutic Agents Using Nanocarriers to Overcome Cancer Resistance. *Nano Today* **2012**, *7*, 367−379.
(5) Song, N.; Yang, Y. W. Molecular and Supramolecular Switches on Mesoporous Silica Nanoparticles. *Chem. Soc. Rev.* **2015**, *44*, 3474−3504.
(6) Ambrogio, M. W.; Thomas, C. R.; Zhao, Y. L.; Zink, J. I.; Stoddart, J. F. Mechanized Silica Nanoparticles: A New Frontier in Theranostic Nanomedicine. *Acc. Chem. Res.* **2011**, *44*, 903−913.
(7) Li, Q. L.; Sun, Y. F.; Sun, Y. L.; Wen, J. J.; Zhou, Y.; Bing, Q. M.; Isaacs, L. D.; Jin, Y. H.; Gao, H.; Yang, Y. W. Mesoporous Silica Nanoparticles Coated by Layer-by-Layer Self-assembly Using Cucurbit[7]uril for *in Vitro* and *in Vivo* Anticancer Drug Release. *Chem. Mater.* **2014**, *26*, 6418−6431.
(8) Zhang, Q.; Wang, X. L.; Li, P. Z.; Nguyen, K. T.; Wang, X. J.; Luo, Z.; Zhang, H. C.; Tan, N. S.; Zhao, Y. L. Biocompatible, Uniform, and Redispersible Mesoporous Silica Nanoparticles for Cancer-Targeted Drug Delivery *in Vivo*. *Adv. Funct. Mater.* **2014**, *24*, 2450−2461.
(9) Wu, Z. L.; Song, N.; Menz, R.; Pingali, B.; Yang, Y. W.; Zheng, Y. B. Nanoparticles Functionalized with Supramolecular Host-Guest Systems for Nanomedicine and Healthcare. *Nanomedicine (London, U. K.)* **2015**, *10*, 1493−1514.
(10) Xue, M.; Zhong, X.; Shaposhnik, Z.; Qu, Y. Q.; Tamanoi, F.; Duan, X. F.; Zink, J. I. pH-Operated Mechanized Porous Silicon Nanoparticles. *J. Am. Chem. Soc.* **2011**, *133* (23), 8798−8801.
(11) Popat, A.; Ross, B. P.; Liu, J.; Jambhrunkar, S.; Kleitz, F.; Qiao, S. Z. Enzyme-Responsive Controlled Release of Covalently Bound Prodrug from Functional Mesoporous Silica Nanospheres. *Angew. Chem., Int. Ed.* **2012**, *51*, 12486−12489.
(12) Barat, R.; Legigan, T.; Tranoy-Opalinski, I.; Renoux, B.; Peraudeau, E.; Clarhaut, J.; Poinot, P.; Fernandes, A. E.; Aucagne, V.; Leigh, D. A.; Papot, S. A Mechanically Interlocked Molecular System Programmed for the Delivery of an Anticancer Drug. *Chem. Sci.* **2015**, *6*, 2608−2613.
(13) Tan, L. L.; Li, H.W.; Qiu, Y. C.; Chen, D. X.; Wang, X.; Pan, R. Y.; Wang, Y.; Zhang, S. X. A.; Wang, B.; Yang, Y. W. Stimuli-Responsive Metal−Organic Frameworks Gated by Pillar[5]arene Supramolecular Switches. *Chem. Sci.* **2015**, *6*, 1640−1644.
(14) Wang, M. D.; Chen, T.; Ding, C. D.; Fu, J. J. Mechanized Silica Nanoparticles Based on Reversible Bistable[2]Pseudorotaxanes as Supramolecular Nanovalves for Multistage pH-Controlled Release. *Chem. Commun.* **2014**, *50*, 5068−5071.
(15) Chen, T.; Yang, N. W.; Fu, J. J. Controlled Release of Cargo Molecules from Hollow Mesoporous Silica Nanoparticles Based on Acid and Base Dual-Responsive Cucurbit[7]uril Pseudorotaxanes. *Chem. Commun.* **2013**, *49*, 6555−6557.
(16) Qiu, X. L.; Li, Q. L.; Zhou, Y.; Jin, X. Y.; Qi, A. D.; Yang, Y. W. Sugar and pH Dual-Responsive Snap-top Nanocarriers Based on Mesoporous Silica-coated Fe_3O_4 Magnetic Nanoparticles for Cargo Delivery. *Chem. Commun.* **2015**, *51*, 4237−4240.
(17) Wu, Y. H.; Long, Y. B.; Li, Q. L.; Han, S. Y.; Ma, J. B.; Yang, Y. W.; Gao, H. Layer-by-Layer (LBL) Self-Assembled Biohybrid Nanomaterials for Efficient Antibacterial Applications. *ACS Appl. Mater. Interfaces* **2015**, *7*, 17255−17263.
(18) Luo, Z.; Cai, K. Y.; Hu, Y.; Li, J. H.; Ding, X. W.; Zhang, B. L.; Xu, D. W.; Yang, W. H.; Liu, P. Redox-Responsive Molecular Nanoreservoirs for Controlled Intracellular Anticancer Drug Delivery Based on Magnetic Nanoparticles. *Adv. Mater.* **2012**, *24*, 431−435.
(19) Guardado-Alvarez, T. M.; Sudha Devi, L.; Russell, M. M.; Schwartz, B. J.; Zink, J. I. Activation of Snap-Top Capped Mesoporous Silica Nanocontainers Using Two Near-Infrared Photons. *J. Am. Chem. Soc.* **2013**, *135*, 14000−14003.
(20) Yan, H.; Teh, C.; Sreejith, S.; Zhu, L. L.; Kwok, A.; Fang, W. Q.; Ma, X.; Nguyen, K. T.; Korzh, V.; Zhao, Y. L. Functional Mesoporous Silica Nanoparticles for Photothermal-Controlled Drug Delivery *in Vivo*. *Angew. Chem., Int. Ed.* **2012**, *51*, 8373−8377.
(21) Li, H.; Tan, L. L.; Jia, P.; Li, Q. L.; Sun, Y. L.; Zhang, J.; Ning, Y. Q.; Yu, J. H.; Yang, Y. W. Near-Infrared Light-Responsive Supramolecular Nanovalve based on Mesoporous Silica-coated Gold Nanorods. *Chem. Sci.* **2014**, *5*, 2804−2808.
(22) Luo, Z.; Ding, X. W.; Hu, Y.; Wu, S. J.; Xiang, Y.; Zeng, Y. F.; Zhang, B. L.; Yan, H.; Zhang, H. C.; Zhu, L. L.; Liu, J. J.; Li, J. H.; Cai, K. Y.; Zhao, Y. L. Engineering a Hollow Nanocontainer Platform with Multifunctional Molecular Machines for Tumor-Targeted Therapy *in Vitro* and *in Vivo*. *ACS Nano* **2013**, *7*, 10271−10284.
(23) Tan, L. L.; Li, H. W.; Zhou, Y.; Zhang, Y. Y.; Feng, X.; Wang, B.; Yang, Y. W. Zn^{2+}-Triggered Drug Release from Biocompatible Zirconium MOFs Equipped with Supramolecular Gates. *Small* **2015**, *11*, 3807−3813.
(24) Wang, C.; Li, Z. X.; Cao, D.; Zhao, Y. L.; Gaines, J. W.; Bozdemir, O. A.; Ambrogio, M. W.; Frasconi, M.; Botros, Y. Y.; Zink, J. I.; Stoddart, J. F. Stimulated Release of Size-Selected Cargos in Succession from Mesoporous Silica Nanoparticles. *Angew. Chem., Int. Ed.* **2012**, *51*, 5460−5465.
(25) Zhou, S. W.; Sha, H. Z.; Liu, B. R.; Du, X. Z. Integration of Simultaneous and Cascade Release of Two Drugs into Smart Single Nanovehicles Based on DNA-Gated Mesoporous Silica Nanoparticles. *Chem. Sci.* **2014**, *5*, 4424−4433.
(26) Gimenez, C.; Climent, E.; Aznar, E.; Martinez-Manez, R.; Sancenon, F.; Marcos, M. D.; Amoros, P.; Rurack, K. Towards Chemical Communication between Gated Nanoparticles. *Angew. Chem., Int. Ed.* **2014**, *53*, 12629−12633.
(27) Croissant, J.; Zink, J. I. Nanovalve-Controlled Cargo Release Activated by Plasmonic Heating. *J. Am. Chem. Soc.* **2012**, *134*, 7628−7631.
(28) Yan, Q.; Zhang, H. J.; Zhao, Y. CO_2-Switchable Supramolecular Block Glycopolypeptide Assemblies. *ACS Macro Lett.* **2014**, *3*, 472−476.
(29) Park, C.; Oh, K.; Lee, S. C.; Kim, C. Controlled Release of Guest Molecules from Mesoporous Silica Particles Based on a pH-Responsive Polypseudorotaxane Motif. *Angew. Chem., Int. Ed.* **2007**, *46*, 1455−1457.
(30) Ferris, D. P.; Zhao, Y. L.; Khashab, N. M.; Khatib, H. A.; Stoddart, J. F.; Zink, J. I. Light-Operated Mechanized Nanoparticles. *J. Am. Chem. Soc.* **2009**, *131*, 1686−1688.
(31) Xiao, Y.; Wang, T.; Cao, Y.; Wang, X.; Zhang, Y.; Liu, Y. L.; Huo, Q. S. Enzyme and Voltage Stimuli-Responsive Controlled Release System based on β-Cyclodextrin-capped Mesoporous Silica Nanoparticles. *Dalton Trans.* **2015**, *44*, 4355−4361.
(32) Wang, T.; Wang, M. D.; Ding, C. D.; Fu, J. J. Mono-Benzimidazole Functionalized β-cyclodextrins as Supramolecular Nanovalves for pH-Triggered Release of *p*-coumaric Acid. *Chem. Commun.* **2014**, *50*, 12469−12472.
(33) Harada, A.; Takashima, Y.; Nakahata, M. Supramolecular Polymeric Materials via Cyclodextrin−Guest Interactions. *Acc. Chem. Res.* **2014**, *47*, 2128−2140.
(34) Feng, A. C.; Yan, Q.; Zhang, H. J.; Peng, L.; Yuan, J. Y. Electrochemical Redox Responsive Polymeric Micelles Formed from Amphiphilic Supramolecular Brushes. *Chem. Commun.* **2014**, *50*, 4740−4742.
(35) Casas-Solvas, J. M.; Ortiz-Salmeron, E.; Fernandez, I.; Garcia-Fuentes, L.; Santoyo-Gonzalez, F.; Vargas-Berenguel, A. Ferrocene-β-Cyclodextrin Conjugates: Synthesis, Supramolecular Behavior, and Use as Electrochemical Sensors. *Chem. - Eur. J.* **2009**, *15*, 8146−8162.
(36) Nakahata, M.; Takashima, Y.; Yamaguchi, H.; Harada, H. Redox-Responsive Self-Healing Materials Formed from Host-Guest Polymers. *Nat. Commun.* **2011**, *2*, 511−516.
(37) Zhang, Z. B.; Luo, Y.; Chen, J. Z.; Dong, S. Y.; Yu, Y. H.; Ma, Z.; Huang, F. H. Formation of Linear Supramolecular Polymers that is Driven by C-H···π Interactions in Solution and in the Solid State. *Angew. Chem., Int. Ed.* **2011**, *50*, 1397−1401.

DOI: 10.1021/acsami.5b05619
ACS Appl. Mater. Interfaces 2015, 7, 21295−21304

(38) Wang, F.; Zhang, J. Q.; Ding, X.; Dong, S. Y.; Liu, M.; Zheng, B.; Li, S. J.; Wu, L.; Yu, Y. H.; Gibson, H. W.; Huang, F. H. Metal Coordination Mediated Reversible Conversion between Linear and Cross-Linked Supramolecular Polymers. *Angew. Chem., Int. Ed.* **2010**, *49*, 1090−1094.
(39) Huang, X.; Du, X. Z. Pillar[6]arene-Valved Mesoporous Silica Nanovehicles for Multi-responsive Controlled Release. *ACS Appl. Mater. Interfaces* **2014**, *6*, 20430−20436.
(40) Sun, Y. L.; Yang, Y. W.; Chen, D. X.; Wang, G.; Zhou, Y.; Wang, C. Y.; Stoddart, J. F. Mechanized Silica Nanoparticles Based on Pillar[5]arenes for On-Command Cargo Release. *Small* **2013**, *9*, 3224−3229.
(41) Fu, J. J.; Chen, T.; Wang, M. D.; Yang, N. W.; Li, S. N.; Wang, Y.; Liu, X. D. Acid and Alkaline Dual Stimuli-Responsive Mechanized Hollow Mesoporous Silica Nanoparticles as Smart Nanocontainers for Intelligent Anticorrosion Coatings. *ACS Nano* **2013**, *7*, 11397−11408.
(42) Sun, Y. L.; Zhou, Y.; Li, Q. L.; Yang, Y. W. Enzyme-Responsive Supramolecular Nanovalves Crafted by Mesoporous Silica Nanoparticles and Choline-Sulfonatocalix[4]arene [2]pseudorotaxanes for Controlled Cargo Release. *Chem. Commun.* **2013**, *49*, 9033−9035.
(43) Lee, J.; Kim, H.; Kim, S.; Lee, H.; Kim, J.; Kim, N.; Park, H. J.; Choi, E. K.; Lee, J. S.; Kim, C. A Multifunctional Mesoporous Nanocontainer with an Iron Oxide Core and a Cyclodextrin Gatekeeper for an Efficient Theranostic platform. *J. Mater. Chem.* **2012**, *22*, 14061.
(44) Zhao, Y. L.; Li, Z. X.; Kabehie, S.; Botros, Y. Y.; Stoddart, J. F.; Zink, J. I. pH-Operated Nanopistons on the Surfaces of Mesoporous Silica Nanoparticle. *J. Am. Chem. Soc.* **2010**, *132*, 13016−13025.
(45) Nguyen, T. D.; Liu, Y.; Saha, S.; Leung, K. C. F.; Stoddart, J. F.; Zink, J. I. Design and Optimization of Molecular Nanovalves Based on Redox-Switchable Bistable Rotaxanes. *J. Am. Chem. Soc.* **2007**, *129*, 626−634.

DOI: 10.1021/acsami.5b05619
ACS Appl. Mater. Interfaces 2015, 7, 21295−21304